Kinetics of Oxidation of Copper Sulfide

V. V. V. N. S. RAMAKRISHNA RAO AND K. P. ABRAHAM

The oxidation rate of a cuprous sulfide pellet suspended in a stream of air was followed by measuring the evolution of SO_2 titrimetrically. Thin thermocouples embedded in the center of the sample recorded the variation of temperature during oxidation. The reaction was found to be topochemical and the sample temperature was found to be higher than its surroundings initially for about half an hour. After this initial period, the sample temperature decreased to that of the surroundings and remained constant during the rest of the period of over 5 hr. The apparent activation energy from the experimental data was found to be different for the initial (nonisothermal) and subsequent (isothermal) periods. Rate controlling mechanisms for these two intervals have been proposed based on interface chemical reaction, mass transfer resistance, and heat transfer concepts. Fair agreement is found between the theoretical rates based on transport mechanisms and those obtained experimentally.

SEVERAL investigators,[1-5] have studied the oxidation of copper sulfides and it has been generally agreed that in the temperature range 750° to 950°C, the oxidation of cuprous sulfide can be represented as

$$Cu_2S + 1\tfrac{1}{2}\,O_2 = Cu_2O + SO_2 \qquad [1]$$

$$\Delta F^\circ_{850^\circ C} = -64{,}850 \text{ cal}$$

followed by

$$Cu_2O + \tfrac{1}{2}\,O_2 = 2CuO \qquad [2]$$

$$\Delta F^\circ_{850^\circ C} = -6090 \text{ cal}$$

The Cu-S-O phase stability diagram valid in the temperature range 477° to 677°C has been given by Ingraham.[6] Fig. 1 is a Cu-S-O phase stability diagram drawn, using similar data, at 850°C, the temperature of interest in the present work. From the diagram it is quite evident that Cu_2O must initially form as an intermediate product during the conversion of Cu_2S to CuO. At higher partial pressures of oxygen present in air, Cu_2O is then converted into CuO. This pattern of behavior during roasting has also been observed by both Peretti[1] and Henderson.[2] However, there seems to be some uncertainty regarding the rate-determining step involved in the oxidation. For instance, according to Peretti,[1] a diffusive step involving the diffusion of the reacting gas is rate controlling, whereas Henderson[2] maintains chemical reaction at the interface, viz., formation of Cu_2O, to be the rate-controlling process. McCabe and Morgan,[3] who carried out the oxidation in an atmosphere of oxygen, are in favor of a mechanism involving transport of gases through the porous oxide layer. In all these investigations the temperature of the system studied was taken to be that of the reaction chamber and little attention was paid to the possible temperature difference between the sample and its surroundings.

Recent investigations[7,8] have stressed the importance of the effect of heat transfer on the reaction kinetics in those cases where marked temperature difference between the sample and its surroundings was noticed.

Reaction [1] is highly exothermic and high temperature differences are likely to be set up between the reaction front and its surroundings during roasting. The present work was initiated with a view to studying the possible effect of this heat generation on the reaction mechanism. For this, provision was made for the continuous measurement of the temperature of the actual reacting compact during the course of oxidation. Commercial roasting of cuprous sulfide is carried out in air in the temperature range used in the present work and as such the data obtained are of interest in commercial roasting operations.

It would also appear from the previous work of Razouk *et al.*,[4] that reaction [2] is as fast as, if not faster than, reaction [1]. If reaction [2] were to be slow, the stoichiometry demands a Cu_2O build-up

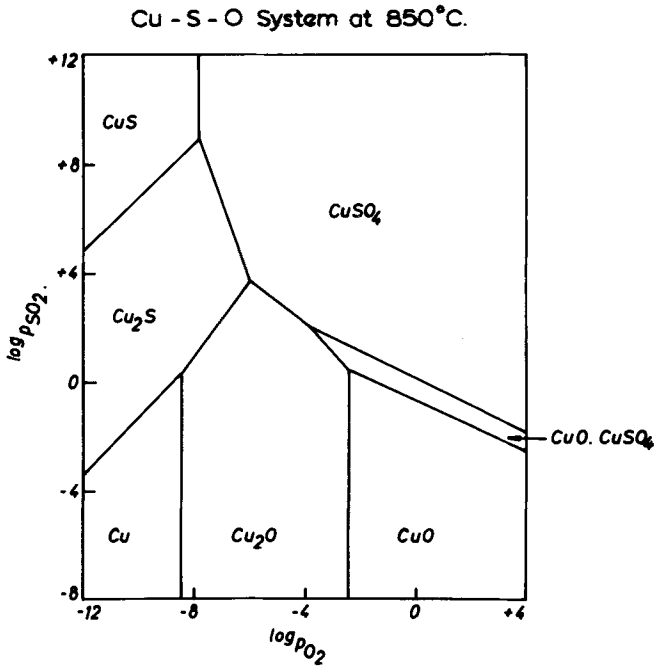

Fig. 1—Cu-S-O phase stability diagram at 850°C.

V. V. V. N. S. RAMAKRISHNA RAO is Senior Scientific Officer, Ministry of Defense, Government of India, and is presently at the Metallurgy Department, Indian Institute of Science, Bangalore, India. K. P. ABRAHAM is Professor, Department of Metallurgy, Indian Institute of Science, Bangalore, India.

Manuscript submitted September 9, 1970.

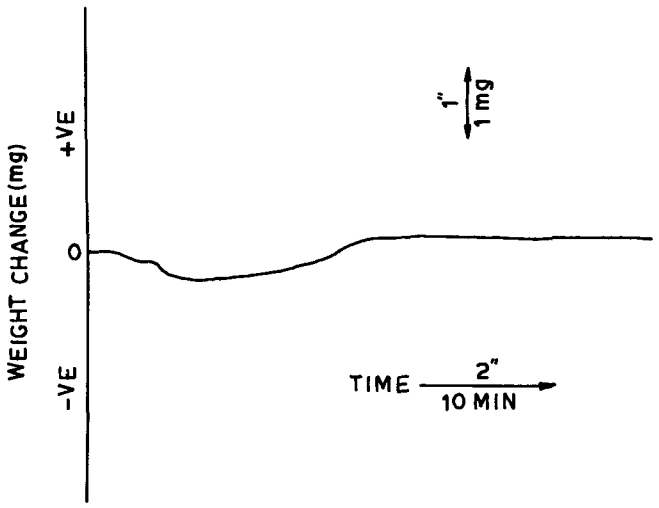

Fig. 2—Thermogram obtained during the initial period of roasting of a Cu_2S compact in air at 850°C.

which should result in a gradual continuous decrease in the weight of the sample throughout the course of oxidation. No such continuous weight loss was observed. Preliminary thermogravimetric experiments carried out by the present authors also confirmed the absence of a major Cu_2O build-up. This can be seen from Fig. 2 which is thermogram obtained by roasting a 400 mg compact of Cu_2S using a recording thermobalance at 850°C. After an initial small loss in weight corresponding to the formation of a thin layer of Cu_2O, there was no further loss in weight, thus confirming the absence of a major Cu_2O build-up.

In order to determine the sample temperature, thermocouple junctions made of thin wires, were embedded in the samples roasted and an automatic recording thermoelectric pyrometer was used to register continuously the temperatures of the furnace, the sample, and its surroundings.

The progress of the oxidation reaction was followed titrimetrically,[5] by estimating the SO_2 liberated during the process. From the geometry of the pellet and the stoichiometry of reaction [1] the following relationship can be obtained for the rate of the reaction in terms of SO_2 evolved

$$r^* = \left[\frac{V_\infty - V_t}{V_\infty}\right]^{1/3}$$

Where r^* represents the dimensionless radius of the reaction front and V_t and V_∞ are the volumes of iodine consumed at time t and at the completion of roasting respectively. In the titrimetric procedure adopted, quantities of SO_2 of the order of 1.6×10^{-4} g could be detected. The results obtained have been analyzed to suggest possible rate-controlling mechanisms.

MATERIALS

Cuprous sulfide supplied by M/s. Albright and Wilson (Mfg) Ltd., London, England, was used in the present work. The finely powdered material was dried in an atmosphere of oxygen-free argon at 110°C before use. The pellets were right cylindrical in form, with a unit height-to-diameter ratio and were made by pressing about 7.0 g of the sulfide in a steel die about

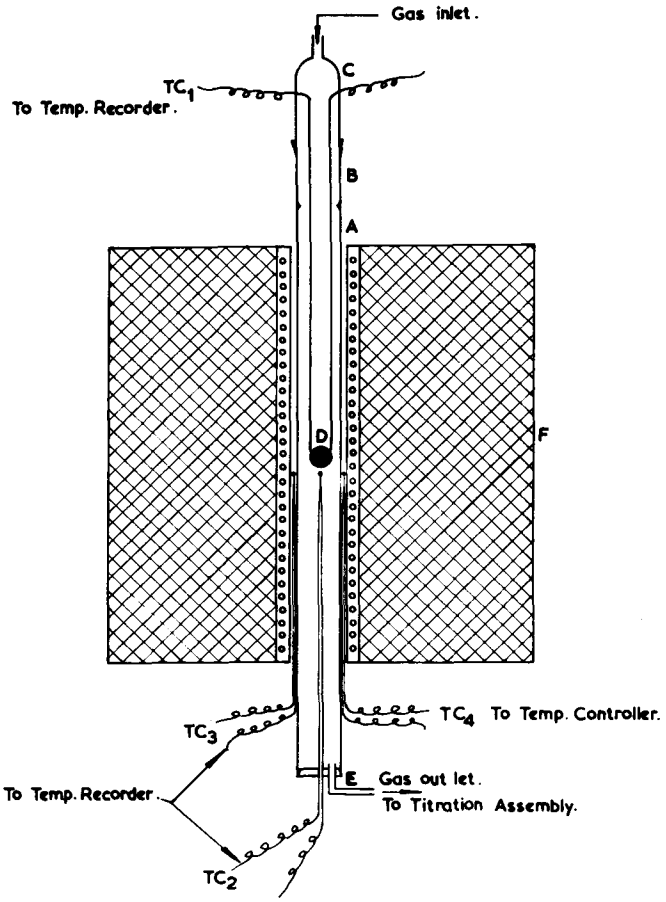

Fig. 3—Experimental assembly.

1.22 cm diam at a pressure of 40 tsi. No binder was used. The pressed pellets had a density equivalent to about 90 pct of the theoretical value. Previous workers also used pellets of similar density.

EXPERIMENTAL

The apparatus used is shown in Fig. 3. The sample was suspended inside the even temperature zone of the furnace, F, by two thin Pt-Pt, 13 pct Rh thermocouple wires (TC_1) whose junction was embedded in the sample and served to measure the reacting compact temperature during the course of the experiment. Thermocouples TC_2 and TC_3 served to measure the temperature of the gas bulk surrounding the reacting compact and that of the furnace, respectively. These three thermocouples, TC_1, TC_2, and TC_3 were connected to a 3-channel recording thermoelectric pyrom eter which recorded continuously the respective temperatures. Thermocouple TC_4 was connected to the electronic temperature controller which controlled the operating temperature within ±4°C.

The gases entered the reaction chamber at the top through the inlet C and SO_2 in the product gases leaving the outlet E was estimated titrimetrically using a decinormal iodine solution, after absorption in distilled water.

The sample was brought to the experimental temperature under purified argon which was then replaced by a stream of dry air.

All oxidation experiments were carried out in air at

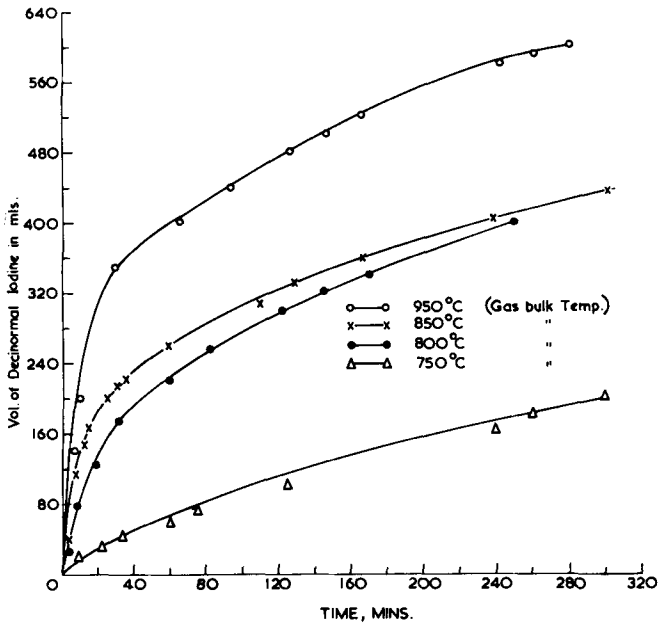

Fig. 4—Plot showing the progress of oxidation of the Cu_2S pellet in terms of the iodine solution consumed.

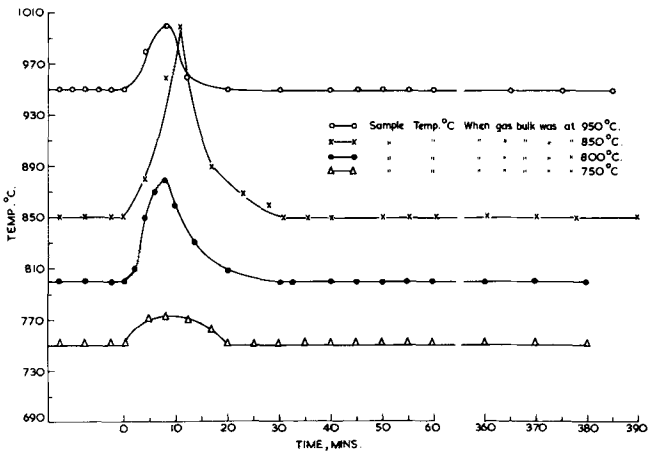

Fig. 5—The rise in temperature of the sample during roasting due to exothermic heat generated, at various temperatures of roasting.

a flow rate of 500 ml per min and, at this flow rate, the reaction rate was found to be independent of the gas flow rate, thus ensuring the absence of gas starvation.

RESULTS

The results are shown in graphical form in Fig. 4, where the progress of the oxidation reaction, at the temperatures mentioned, is represented in terms of the volume of the decinormal iodine reacted with the liberated sulfur dioxide.

It was also observed that during the initial period the sample temperature was much higher than its surroundings. This is shown in Fig. 5. However, at all temperatures the sample temperature levelled off to the temperature of its surroundings after about 20 to 30 min and remained constant during the subsequent oxidation period lasting about 5 hr. At the higher temperatures, about 60 pct of the roasting was over in about 6 hr whereas, at 750°C, as little as 15 pct oxidation took place during the period.

Sectioning of the partially roasted specimens confirmed that, in the temperature range of interest, the reaction was always topochemical. A photomicrograph of a partially roasted pellet of Cu_2S after sectioning is shown in Fig. 6. It can be seen that the central core of unreacted Cu_2S is covered by a thin layer of Cu_2O followed by a thick layer of CuO. The various phases were identified both by chemical analysis and also by taking X-ray diffraction patterns. The X-ray patterns taken with filtered copper radiation showed the presence of CuO as the major constituent and Cu_2S as the second major constituent with small quantities of Cu_2O present.

DISCUSSION

The possible rate controlling steps in the oxidation of Cu_2S pellets in a stream of dry air may be grouped as follows:-

i) diffusion of the reactant and the product gases through the gas film surrounding the sample,

ii) diffusion of these gases through the porous oxide layer (also intraparticle diffusion, if any), and

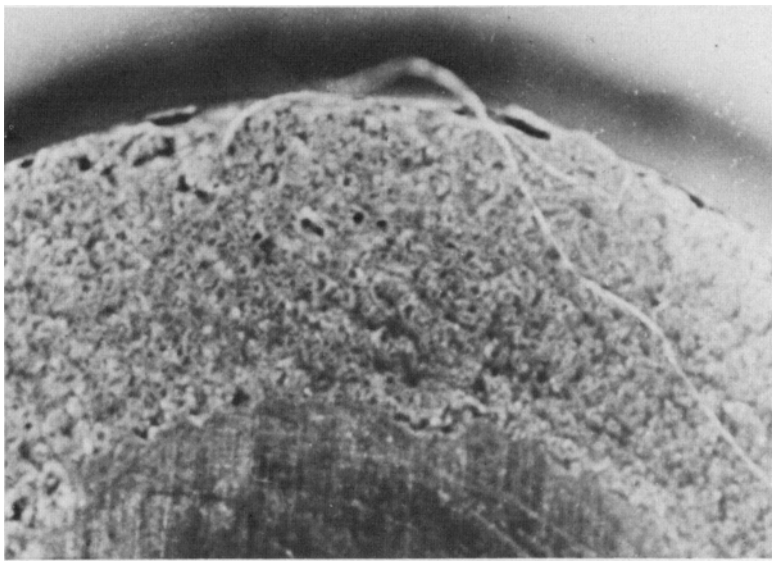

Fig. 6—Section of a partially roasted Cu_2S sample.

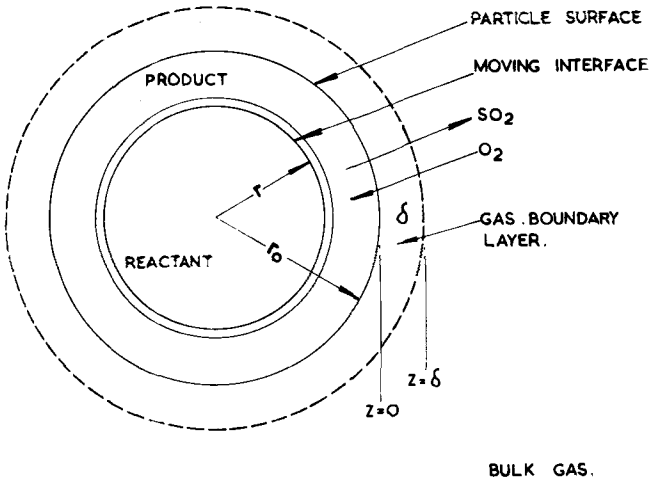

Fig. 7—Schematic diagram representing the oxidation of a cuprous sulfide pellet.

iii) chemical reaction at an interface as given by Eq. [1]. Eq. [2] is not considered for the reason already given earlier. This is initiated at the surface of the sample at zero time, and the reacting interface recedes towards the center of the sample with time as the oxidation progresses.

It would appear that, in the initial period when the product layer is not sufficiently thick, the reaction at the interface is likely to be the rate-controlling step, to be followed by the diffusion-controlled process as the layer is built up.

In addition, if the temperature of the sample is substantially different from its surroundings, heat transfer effects have to be taken into consideration while deciding the rate-controlling step.

In the treatment which follows, the experimental results have been analyzed separately for the initial (nonisothermal) and the subsequent (isothermal) intervals.

CHEMICAL REACTION AS THE RATE-CONTROLLING FACTOR IN THE INITIAL PERIOD

A schematic diagram representing the topochemical oxidation of the Cu_2S compact (right cylindrical with height equal to diameter) in air according to Eq. [1] is shown in Fig. 7. The reaction as represented by Eq. [1] occurs at the interface separating the solid Cu_2S and the product Cu_2O phases. This interface moves inwards from the surface of the compact as the reaction proceeds. Taking into account the conservation of the original solid species, the rate of change of its radius can be expressed in terms of the molar reaction rate by the following equation*

*All nomenclature is defined at the end of the paper.

$$\dot{n} = -6\pi r^2 \rho \frac{dr}{dt} \qquad [3]$$

For the oxidation reaction under consideration the forward reaction rate is proportional to the rate of absorption of the reactant gas and the backward reaction rate is proportional to the rate of reabsorption of the product gas. Expressing mathematically,

$$n_f = K_f / R\theta_G [p_{O_2}]_G \qquad [4]$$

and

$$n_b = K_b / R\theta_G [p_{O_2}]_G \qquad [5]$$

The net reaction rate $n = (n_f - n_b)$

$$= \frac{1}{R\theta_G} \{K_f [p_{O_2}]_G - K_b [p_{SO_2}]_G\} \qquad [6]$$

At equilibrium

$$K_f [p_{O_2}]_{eq} = K_b [p_{SO_2}]_{eq} \qquad [7]$$

But

$$[p_{SO_2}]_{eq} / [p_{O_2}]_{eq} = K_{eq} = \frac{K_f}{K_b} \qquad [8]$$

Thus the net reaction rate can be written as

$$n = \frac{K_f}{R\theta_G} \{[p_{O_2}]_G - [p_{SO_2}]_G / K_{eq}\} \qquad [9]$$

This K_f is the same as k_c, the chemical rate constant. Reaction rate over the area of the reaction surface will then be

$$\dot{n} = 6\pi r^2 \frac{K_c}{R\theta_G} \{[p_{O_2}]_G - [p_{SO_2}]_G / K_{eq}\} \qquad [10]$$

Combining Eqs. [3] and [10] the resulting differential equation can be solved to get the rate of advance of the reaction front per unit surface area. Remembering that $[p_{SO_2}]_G / K_{eq} \ll [p_{O_2}]_G$ since K_{eq} is very large, we get

$$r_0 \rho (1 - r^*) = \frac{K_c}{R\theta_G} [p_{O_2}]_G t \qquad [11]$$

and hence a plot of the expression on the left-hand side of Eq. [11] with time t should result in a straight line. Fig. 8 is a plot of such a relation obtained at 850°C. Two distinct regions are seen: an approximate straight line during the nonisothermal initial period, followed by a parabolic curve pertaining to the isothermal interval. A particle temperature vs time plot, corresponding to the experimental temperature of 850°C is also shown in the same Fig. 8.

Apparent activation energies for the oxidation proc-

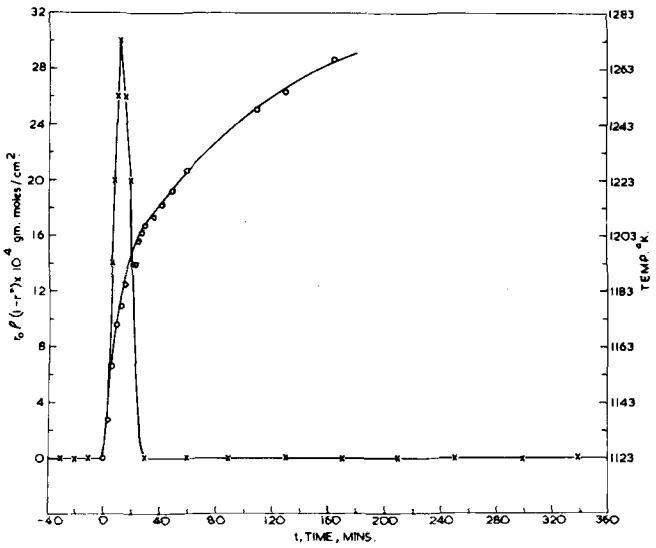

Fig. 8—Experimental plot of $r_0 \rho (1 - r^*)$ against time for a cuprous sulfide pellet reacting in air at 850°C. The variation of the sample temperature with time is also indicated (x-x-x-x).

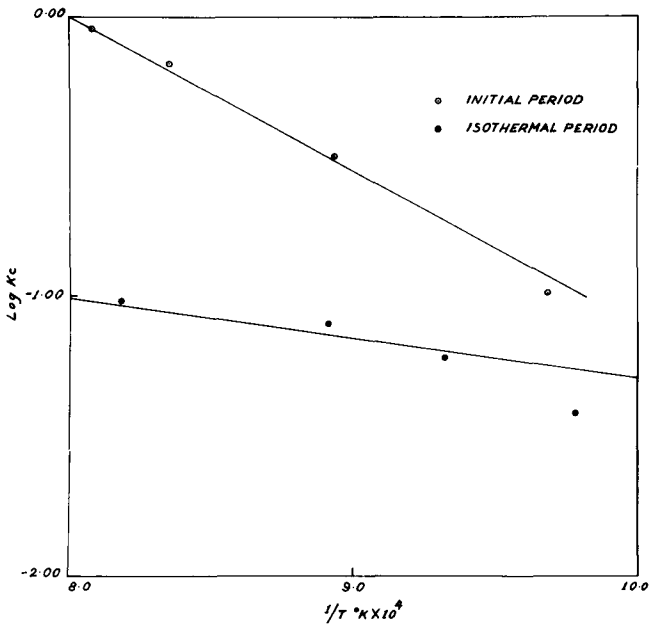

Fig. 9—The Arrhenius plot for calculating the apparent activation energies.

ess can be calculated from the progress of oxidation observed at the different experimental temperatures. Fig. 9 is the Arrhenius plot corresponding to the initial nonisothermal and the subsequent isothermal periods. The activation energies which can be calculated were found to be of the order of 25.0 kcal per g-mole and 6.0 kcal per g-mole, for the initial and subsequent periods respectively.

The high activation energy and an approximate linear nature of the plot in Fig. 8 during the initial period is suggestive of a chemical control mechanism in this interval. However, these characteristics are also true of processes controlled by heat and mass transfer.[7] Therefore, during the initial period the mechanism of oxidation could involve the heat and mass transfer through the porous product and boundary layers and/or chemical reaction at the interface.

Since the particle temperature was found to be significantly higher than the surroundings and a high activation energy has also been obtained, the rate of advance of the reaction front should vary rapidly with time during this period if it were to be an exclusively chemically controlled process. However, it is seen from Fig. 8 that the reaction front velocity is not substantially deviating from linearity.

Further, with the release of the exothermic heat at the reaction front resulting in higher temperatures, the reaction rate should continuously increase for a chemically controlled process. Instead, a tendency for the reaction rate to decrease is observed after a few minutes from the start of the reaction. It can be concluded therefore that chemical reaction is not rate controlling but that the reaction is likely to be controlled by a transport mechanism. Even when the diffusive steps are likely to be rate controlling the diffusivities are no doubt increased by the higher sample temperature generated by the exothermic heat, however, the higher diffusivities do not cause higher reaction rate because of the increase in the diffusional resistance as a result of the progressive increase in the thickness of the product layer.

The experimental data obtained are therefore analyzed on the basis of mass and heat transfer concepts. For this, again, the results obtained at 850°C are used because the maximum temperature difference between the compact and its surroundings was noted at this temperature.

EFFECT OF DIFFUSION AND MASS TRANSFER

Even though a moving interface is involved in the present topochemical oxidation process, the analysis assumes a quasi-steady state process. This assumption is justified in view of the fact that only an infinitesimally small fraction of the total flux diffusing is likely to be accumulating, if at all, within the pores of the product mass.

Assuming chemical equilibrium at the reaction front, a rate equation for the nonisothermal period can be written in the form given below. The mass transfer of both product and reactant gases are taken into account and the procedure adopted is similar to that used by Hills.[7]

$$\dot{n} = \frac{[p_{O_2}]_G - [p_{SO_2}]_G/K_{eq}}{R\theta_G \left[\frac{[\Omega_M]_{II}}{K_{eq}} + \frac{3}{2}[\Omega_M]_I\right]} \qquad [12]$$

where $[\Omega_M]_I$ and $[\Omega_M]_{II}$ represent the mass transfer resistances due to both porous product layer and boundary layer relevant to the reactant and product gases, respectively.

Since the K_{eq} in the present case is very large and of the order of 10^{12} (at 850°C) and $[\Omega_M]_I$ and $[\Omega_M]_{II}$ are both small and of equal order, Eq. [12] can be approximated to

$$\dot{n} = \frac{[p_{O_2}]_G}{R\theta_G \cdot \frac{3}{2}[\Omega_M]_I} \qquad [13]$$

Expanding $[\Omega_M]_I$ and rewriting Eq. [13] gives*

*Though D_{eff} varies with temperature, it is assumed that the ratio θ/D_{eff} varies little and that errors arising from this assumption are therefore negligible.

$$\dot{n} = \frac{[p_{O_2}]_G}{\frac{R\theta_G}{4\pi[D_{eff}]_I r_0}\left\{\left(\frac{1}{r^*} - 1\right) + \frac{[D_{eff}]_I}{\alpha_I r_0}\right\}} \qquad [14]$$

The experimental rate can now be compared with the theoretical rate obtainable from Eq. [14].

The initial experimental rate could be determined from Fig. 4 and the theoretical value from Eq. [14] above, provided effective diffusivity, $[D_{eff}]_I$ and mass transfer coefficient $[\alpha]_I$ are known.

The mass transfer coefficient can be calculated from the equations suggested by Rowe, Claxton, and Lewis[9] and Ranz and Marshall,[10] the results being expressed in terms of dimensionless correlations of the form

$$\alpha = \frac{[D]_G}{d}[2 + f(\mathrm{Re}, \mathrm{Sc})] \qquad [15]$$

Similarly the diffusion coefficient in the gas phase, $[D]_G$ can be estimated from empirical equations such as those of Gilliland and Hirshfelder and coworkers.[11]

Table I. Determination of the Mass Transfer and Effective Diffusion Coefficients

Diameter of the reaction tube	4 cm
Air flow rate through the reaction tube	500 ml per min
Diameter of the reacting compact (d)	1.223 cm
Sherwood number (Sh)	2.64
Diffusivity of the reactant gas in the bulk gas phase $[D_G]_{I,\ 850°C}$ (from Gilliland)[11]	0.83 cm^2 per sec
Mass transfer coefficient to the surface of the reacting compact $[\alpha]_{I,\ 850°C}$	2.40 cm per sec
Porosity of the porous oxide layer	0.25
Tortuosity factor	3.0
Effective diffusivity of the reactant gas in the porous oxide layer $[D_{eff}]_I$	0.017 cm^2 per sec

Table II. Comparison Between the Experimental and the Theoretical Reaction Rates, at the Experimental Temperature 850°C

	Reaction Rate in g Mole per sec	
Time in Minutes	Theoretical	Experimental
3	1.07×10^{-5}	1.20×10^{-5}
8	5.00×10^{-6}	8.0×10^{-6}
12	3.76×10^{-6}	5.0×10^{-6}
18	3.22×10^{-6}	3.3×10^{-6}

Toor[12] has shown that these equations are also relevant to the type of gaseous diffusion encountered under the present experimental conditions.

The effective diffusivity, D_{eff} is then obtained from this $[D]_G$, using the relation described by Wakao and Smith.[13]

$$D_{eff} = \frac{[D]_G \gamma^2}{\tau} \qquad [16]$$

This equation is used in view of the bidisperse structure[14] of pores in the product layer of the reacting compact as revealed by the microscopic examination.

While the porosity factor, γ, can be estimated with reasonable accuracy, there is some uncertainty regarding the correct value of the tortuosity factor, τ, which is an empirical correlation factor to allow for both tortuosity and varying pore cross section.

In view of the high pressures used in compacting and the low porosity observed, a tortuosity factor of 3 appears to be reasonable and has been used in the present calculations. The values of $[\alpha]_I$ and $[D_{eff}]_I$ calculated from Eqs. [15] and [16] are presented in Table I. Using these values in Eq. [14], the theoretical reaction rate at various initial time intervals can be calculated on the basis of the mass transfer resistance concept.

In Table II the theoretical rates are compared with those obtained experimentally for the corresponding time intervals. It is seen from Table II that the theoretical rates are in satisfactory agreement with the experimental rates and that the latter values are never lower than their corresponding theoretical estimates.

From this it can be concluded that the chemical reaction at the interface cannot play any significant role in determining the rate of the reaction.

Effect of Heat Transfer

In view of the high temperature rise in the reacting compact during the initial period of oxidation, heat transfer phenomenon may also be important in the rate controlling mechanism. Consequently the experimental data has to be correlated with an equation based on the heat transfer process.

Table III. Comparison of the Experimental and Theoretical Reaction Rates

	Reaction rates in g-mole per sec		
	Theoretical		
Time Minutes	Based on Eq. [14] (Diffusion and Mass Transfer Controlled)	Based on Eq. [19] (Heat Transfer Controlled)	Experimental
3	1.07×10^{-5}	1.068×10^{-5}	1.20×10^{-5}
8	5.00×10^{-6}	3.872×10^{-5}	8.00×10^{-6}
12	3.76×10^{-6}	5.253×10^{-5}	5.00×10^{-6}
18	3.22×10^{-6}	1.221×10^{-5}	3.30×10^{-6}

Heat is generated at the reaction front as a result of the exothermic nature of the oxidation process

$$\dot{q} = \dot{n}H \qquad [17]$$

Considering the heat transfer by conduction, convection and radiation through the porous product layer and the outer boundary layer on quasi-steady state terms, a simplified equation can be written for $\dot{q}$

$$\dot{q} = \frac{(\theta_R - \theta_G)}{\frac{1}{6\pi r_0 k}\left[\left(\frac{1}{r^*} - 1\right) + \frac{k}{h r_0}\right]} \qquad [18]$$

Combining Eqs. [17] and [18]

$$\dot{n} = \frac{(\theta_R - \theta_G)}{\frac{H}{6\pi k r_0}\left[\left(\frac{1}{r^*} - 1\right) + \frac{k}{h r_0}\right]} \qquad [19]$$

The temperature indicated by the thermocouple embedded at the center of the sample is assumed to be the reaction interface temperature and the reaction rate, $\dot{n}$, can be calculated from Eq. [19] if the values of K, the thermal conductivity of the product solid, and h, the total heat transfer coefficient ($h = h_{convection} + h_{radiation}$), are known. $h_{convection}$ can be calculated from the Ranz and Marshall correlation of the type.

$$\frac{h_{conv.}\, d}{k_G} = 2 + 0.6\,(Re)^{1/2}(Pr)^{1/3} \qquad [20]$$

A fairly accurate value for the radiation heat transfer coefficient, $h_{radiation}$, can be obtained by approximating the furnace to an enclosure whose surface area is very much greater than that of the sample, and it can be shown[15] that

$$h_{rad} = \sigma\epsilon(\theta_W^2 + \theta_S^2)(\theta_W + \theta_S) \qquad [21]$$

Substituting the relevant values in Eq. [19], the rate of the reaction, $\dot{n}$, can be obtained at various time intervals.

In Table III are presented the reaction rates theoretically obtained from Eq. [19] along with the corresponding values obtained experimentally. The theoretical rates based on the diffusion and mass transfer rate Eq. [14] are also included here for the sake of completeness. It is seen from Table III that the reaction is controlled by heat and mass transfer at the beginning of the oxidation process and thereafter the heat transfer effect becomes less important due to the ever-increasing oxide layer formation and as a result the diffusive steps become solely responsible for the rate controlling mechanism.

This conclusion is corroborated by the analysis of the experimental results pertaining to the isothermal oxidation period shown in the next section.

Mechanism During the Isothermal Period

The nonlinearity of the plot in the isothermal region shown in Fig. 8, together with the small value of the apparent activation energy, can be taken as positive indications for the transport controlled mechanism during this period. Eq. [13] is still valid in this period where $[\Omega_M]_I$ stands for the total mass transfer resistance offered to the diffusion of the reactant gas from the bulk to the reaction front. This resistance $[\Omega_M]_I$ can however be split into three components at the beginning of the isothermal period, as

i) the resistance offered by the outer boundary layer,

$$\frac{1}{6\pi r_0^2 [\alpha]_I}$$

ii) a constant resistance offered by the product layer of thickness $(r_0 - r_0')$ already formed during the initial nonisothermal period,

$$\frac{r_0 - r_0'}{6\pi r_0 r' [D_{eff}]_I}$$

iii) the resistance offered by the product layer of thickness $(r_0' - r)$ at time t, from the beginning of the isothermal period,

$$\frac{(r_0' - r_0)}{6\pi r_0' r [D_{eff}]_I}$$

Substituting the sum of the above three resistance expressions in place of $[\Omega_M]_I$ in Eq. [13] and rearranging we get,

$$\frac{[p_{O_2}]_G}{\dot{n}} = \frac{R\theta_G}{4\pi[D_{eff}]_I r_0'}\left(\frac{1}{r^{*\prime}} - 1\right) + R\theta_G \frac{1}{4\pi r_0^2 \alpha_I} + \frac{r_0 - r_0'}{4\pi r_0 r_0' [D_{eff}]_I} \qquad [22]$$

According to Eq. [22] a plot of $[p_{O_2}]_G/\dot{n}$ against $(1/r^{*\prime} - 1)$ should be straight line whose slope should give the value of the effective diffusivity, $[D_{eff}]$ and the intercept, the value of the mass transfer coefficient $[\alpha]_I$.

Fig. 10 is such a plot of the values obtained from the results at 850°C. The values of $\dot{n}$ were calculated from experimental data by numerical methods of analysis.[16] The linearity of the plot obtained justifies and confirms the present approach based on transport control and shows that the chemical step at the reaction interface cannot play any significant role in determining the reaction rate.

The experimental values of mass transfer coefficient $[\alpha]_I$, and effective diffusivity $[D_{eff}]_I$, obtained from Fig. 10 are given in Table IV along with their theoretical counterparts estimated from Eqs. [15] and [16] mentioned earlier. It will be seen from Table IV that there is fair agreement between the theroetical and experimental values of $[\alpha]_I$, but the theoretical $[D_{eff}]_I$ is higher than the experimental value by a factor of 2.

This disparity in the values of $[D_{eff}]_I$ may be due partly to the uncertainty involved in the value of tortuosity factor used and partly to the approximate nature of the assumptions made in the relevant calculations. However, it may be of interest to mention that such deviations are not uncommon in investigations of this type.[17]

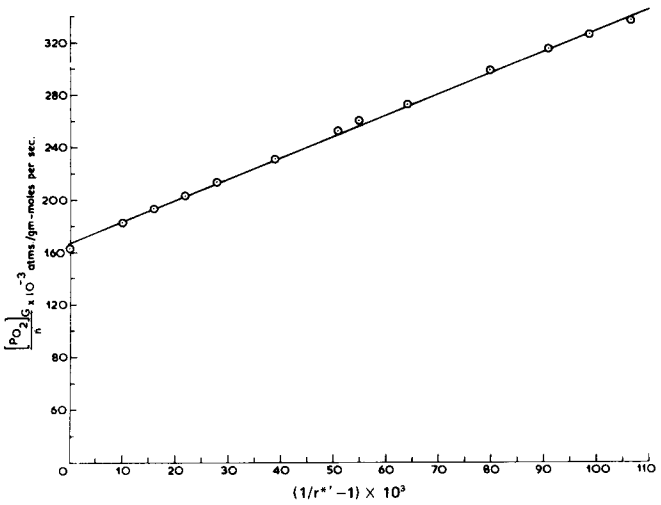

Fig. 10—Experimental plot of $[p_{O_2}]_G/\dot{n}$ against $[(1/r^{*\prime}) - 1]$ for the cuprous sulfide pellet reacting in air at 850°C.

Table IV. Comparison Between Experimental and Theoretical Values for the Transport Properties Calculated at 850°C

Transport Parameter	Experimental	Theoretical
$[D_{eff}]_I$ (cm² sec⁻¹)	0.00824	0.0173
$[\alpha]_I$ (cm sec⁻¹)	1.82	2.40

SUMMARY

1) There was appreciable difference in temperature between the sample and its surroundings when the Cu_2S pellets were roasted in air during the initial period of about half an hour, but the temperature difference leveled off and remained constant during the rest of the period of roasting lasting about 5 hr.

2) The effect of heat transfer on the overall rate was significant at the beginning of the oxidation process when the product layer thickness was small.

3) When the reaction was controlled by heat and mass transfer, the effect of heat transfer was more significant in the boundary layer than in the product mass, while the effect of mass transfer was more pronounced in the product mass than in the boundary layer, as can be seen on substitution of relevant data in Eqs. [19] and [14], respectively.

4) Throughout the oxidation process diffusive steps were found to be rate controlling.

NOMENCLATURE

d	diameter (equal to height) of the cylindrical compact, cm
D	diffusion coefficient, sq cm per sec
D_{eff}	effective diffusion coefficient in the product layer, sq cm per sec
h	heat transfer coefficient, cal per sq cm per sec, °K

H	heat of reaction, cal per g-mole
K	thermal conductivity of product solid, cal per cm per sec, °K
K_b	rate constant for the backward reaction, cm per sec
K_c	chemical rate constant, cm per sec
K_f	rate constant for the forward reaction, cm per sec
k_G	thermal conductivity of gas, cal per cm, per sec, °K
m_0, m_t, m_∞	initial, interim, and final mass, respectively, of reacting compact, g
$\dot{n}$	rate of reaction, g-mole per sec
n	rate of reaction, g-mole per sq cm per sec
n_b	backward reaction rate
n_f	forward reaction rate
p	partial pressure, atm
q	heat transfer rate, cal per sec
r_0	initial radius of reacting compact (equal to half the initial height), cm
r_0'	radius of reaction front at the beginning of the isothermal period, cm
r	radius of reaction front, cm
R	gas constant in mechanical units, cu cm atm per g-mole, °K
R'	gas constant in heat units, cal per g-mole, °K
t	time, sec (unless otherwise stated)
V_G	linear velocity of gas past a reacting compact, cm per sec

Greek Symbols

α	mass transfer coefficient, cm per sec
δ	boundary layer thickness, cm
θ	temperature, °K
μ	viscosity of gas, g per sec, cm
ν	kinematic viscosity of gas, sq cm per sec
ρ	molar density of compact, g-mole per cu cm
σ	Stefan-Boltzman constant, cal per sq cm per sec, °K^4
$[\Omega_M]$	mass transfer resistance, sec per cu cm

Dimensionless Variables

K_{eq}	equilibrium constant
m^*	dimensionless mass of reacting compact, $(m_t - m_\infty)/(m_0 - m_\infty)$
Nu	Nusselt number, hd/k_G
Pr	Prandtl number, $\nu C_b/k_G$
Sc	Schmidt number, ν/D
Sh	Sherwood number, $\alpha d/D_G$
Re	Reynolds number, $V_G d/\nu$
$r^*, r^{*\prime}$	dimensionless radius of reaction front, $r^* = r/r_0$, $r^{*\prime} = r/r_0'$
γ	porosity factor in the porous solid
ϵ	emissivity
τ	tortuosity factor in the porous solid

Suffixes

G	value in gas flowing through the reaction tube
R	value at reaction front
I	value for reactant gas
II	value for product gas
0	value at beginning of reaction
S	value at the surface
W	value at the reactor wall

ACKNOWLEDGMENTS

The authors are grateful to Professor A. A. Krishnan for his interest in the present work. One of the authors (Ramakrishna Rao) expresses his gratitude to Dr. R. V. Tamhankar, Director, Defence Metallurgical Research Laboratory, Hyderabad (A.P.) for his encouragement and to the Government of India, Ministry of Defence for the grant of study leave during which period this investigation was carried out.

REFERENCES

1. E. A. Peretti: *Discussions Faraday Soc.*, 1948, vol. 4, pp. 174-79.
2. T. A. Henderson: *Bull. Inst. Mining Met.*, 1958, vol. 620, pp. 497-520.
3. C. L. McCabe and J. A. Morgan: *Trans. AIME*, 1956, vol. 206, p. 800A.
4. R. I. Razouk, M. Y. Farah, R. S. Mikhail, and G. A. Kolta: *J. Appl. Chem.* (London), 1962, vol. 12, pp. 190-96.
5. M. E. Wadsworth, K. L. Leiter, W. H. Porter, and L. R. Lewis: *Trans. TMS-AIME*, 1960, vol. 218, p. 519.
6. T. R. Ingraham: *Trans. TMS-AIME*, 1965, vol. 223, p. 359.
7. A. W. D. Hills: *Heat and Mass Transfer in Process Metallurgy*, pp. 39-77, The Institute of Mining and Metallurgy, London, 1967.
8. N. J. Themelis and J. C. Yannopoulos: *Trans. TMS-AIME*, 1966, vol. 236, pp. 414-20.
9. P. N. Rowe, K. T. Claxton, and J. B. Lewis: *Trans. Inst. Chem. Engrs.*, 1965, vol. 43, pp. 14-31.
10. W. E. Ranz and W. R. Marshall: *Chem. Eng. Progr.*, 1952, vol. 48, pp. 141-46, 173-80.
11. *Chemical Engineers Handbook*, Fourth ed., J. H. Perry, ed., pp. 14-21, McGraw-Hill Book Co., New York, 1963.
12. H. L. Toor: *A.I.Ch.E. J.*, 1957, vol. 8, p. 198.
13. N. Wakao and J. M. Smith: *Chem. Eng. Sci.*, 1962, vol. 17, p. 825.
14. C. N. Satterfield and T. K. Sherwood: *The Role of Diffusion in Catalysis*, Addison-Wesley, London, 1963.
15. Wm. H. McAdams: Heat Transmission, Third ed., McGraw-Hill Book Co., New York, 1954.
16. Kaj L. Nielsen: *Methods in Numerical Analysis*, Chapter 8, The Macmillan Co., New York, 1961.
17. Norman Steisel and John B. Butt: *Chem. Eng. Sci.*, 1967, vol. 22, p. 469.